# Surface-Controlled Mono/Diselective *ortho* C−H Bond Activation

Qing Li,[‡] Biao Yang,[‡] Haiping Lin,[‡] Nabi Aghdassi, Kangjian Miao, Junjie Zhang, Haiming Zhang, Youyong Li, Steffen Duhm, Jian Fan,* and Lifeng Chi*

Institute of Functional Nano & Soft Materials (FUNSOM), Jiangsu Key Laboratory for Carbon-Based Functional Materials & Devices, Soochow University, 199 Ren'ai Road, Suzhou, 215123, Jiangsu P. R. China

Ⓢ *Supporting Information*

ABSTRACT: One of the most charming and challenging topics in organic chemistry is the selective C−H bond activation. The difficulty arises not only from the relatively large bond-dissociation enthalpy, but also from the poor reaction selectivity. In this work, Au(111) and Ag(111) surfaces were used to address *ortho* C−H functionalization and *ortho-ortho* couplings of phenol derivatives. More importantly, the competition between dehydrogenation and deoxygenation drove the diversity of reaction pathways of phenols on surfaces, that is, diselective *ortho* C−H bond activation on Au(111) surfaces and monoselective *ortho* C−H bond activation on Ag(111) surfaces. The mechanism of this unprecedented phenomenon was extensively explored by scanning tunneling microscopy, density function theory, and X-ray photoelectron spectroscopy. Our findings provide new pathways for surface-assisted organic synthesis via the mono/diselective C−H bond activation.


On Au(111)   On Ag(111)
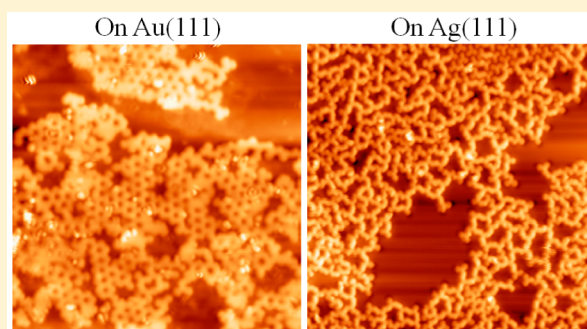
INTRODUCTION

One of the most straightforward pathways to synthesize desirable organic molecules is, in principle, the C−H bond functionalization. Stimulated by this perspective, tremendous effort has been devoted to the scission of C−H bonds in the past decades, involving transition metal catalysis and harsh condition applications.[1] The selective aromatic C−H activation has still been considered one of the most challenging topics in organic chemistry due to the existence of multiple reaction sites.[2] One powerful and widely applied strategy to control the selectivity of C−H activation is to introduce a directing group. So far, impressive success has been achieved in the regioselective aromatic C−H activation via the directing strategy. However, it is still difficult to control the mono- and diselective C−H activations, since two identical C−H bonds are available adjacent to the directing group in the precursor.

Recently, the development of "on-surface chemistry", in which heterogeneous catalysis has been performed on a metal support,[3−15] provides alternative routes for the C−H functionalization. With this technique, the intramolecular aryl−aryl coupling via the cleavage of C−H bonds was realized, and it has been widely utilized for, e.g., the preparation of graphene nanoribbons on metal surfaces.[16−19] Meanwhile, much attention has been paid to the intermolecular aryl−aryl coupling via C−H activation for the synthesis of 0D, 1D, or 2D molecular nanosystems under ultrahigh vacuum (UHV).[20−24] However, although regioselective aromatic C−H activation on surfaces has been investigated by a few research groups,[24] control over the mono- and diselective C−H activations has not been addressed yet.

Herein, with the introduction of hydroxyl as a directing group into two model compounds (1,3,5-tris(4-hydroxyphenyl)benzene (THPB) and 4,4'''-dihydroxy-*p*-quaterphenyl (DHQP), as shown in Scheme 1), we realized regioselective aromatic C−H activations on both gold and silver surfaces. More importantly, surface-controlled mono- and

Scheme 1. (a,b) Schemes of the Reaction Behaviors of THPB and DHQP Precursors, Showing Mono- and Diselective *ortho* C−H Activation on Au(111) and Ag(111), Respectively
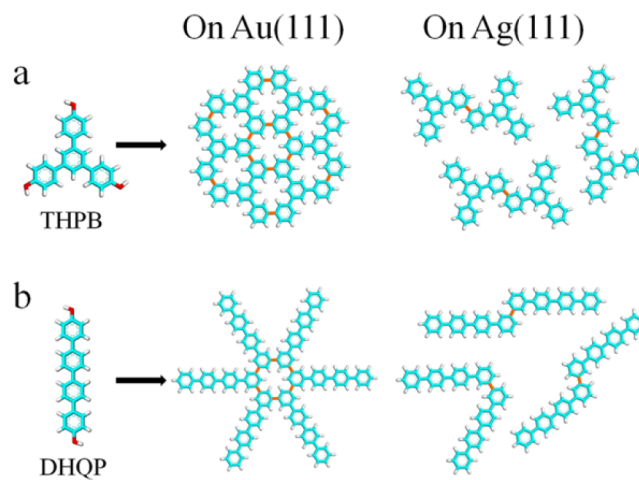
diselective *ortho* C−H bond activation was explored: For THPB and DHQP precursors, both *ortho* C−H bonds are activated on Au(111) surfaces, whereas only one *ortho* C−H bond of each phenol ring is activated on Ag(111) surfaces (Scheme 1). Combining high resolution scanning tunneling microscopy (STM) studies with X-ray photoelectron spectroscopy (XPS) measurements and density functional theory (DFT) calculations, we demonstrate that the surface-controlled mono- and diselectivity of C−H functionalization arises from the binding strength difference between the metal substrates and the phenol oxygen atoms. Considering the excellent selectivity and generality of mono- and di-*ortho* C−H activation, we believe our finding opens doors to a wide range of prospects for the organic synthesis and catalyst development via "on-surface chemistry".

■ RESULTS AND DISCUSSION

THPB molecules form well ordered self-assembly islands propagating on the entire Au(111) surface after depositing at room temperature, in which the individual molecules are distinguishable (Figure S1a). DFT calculations reveal that the constituting molecules adsorb on the surface in a planar conformation and are linked to each other via hydrogen bonding between hydroxyl groups (Figure S1). Samples prepared at higher temperatures (260 °C) show distinctively different structures, as shown in Figure 1a. THPB monomers are still visible occasionally; however, most of the precursors are interconnected, exhibiting an irregular phase, in which no apparent periodicity or orientation can be found. By further increasing the substrate temperature (320 °C) during the deposition, a new phase emerges in addition to the irregular
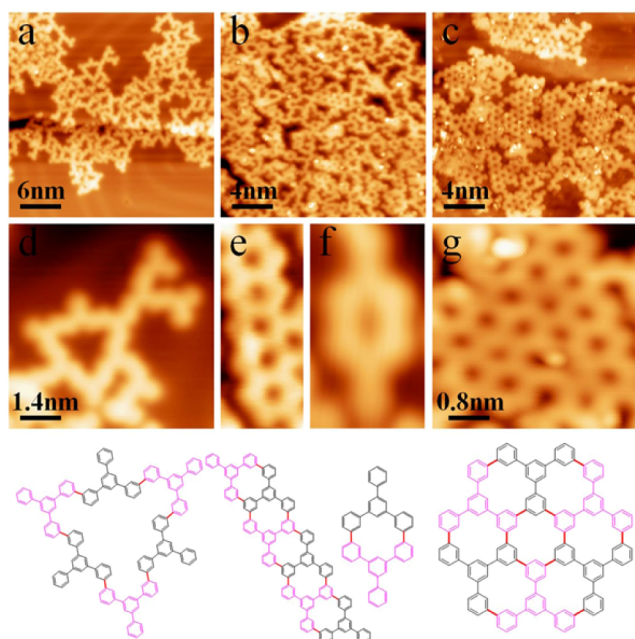

Figure 1. Structural evolutions of THPB on Au(111) surfaces upon thermal annealing. (a−c) Representative STM images for sample preparation temperatures of 260, 320, and 340 °C, respectively. (d−g) Zoomed STM images of (a−c). Structural models for (d−g) are shown in the lower panels. Newly formed C−C bonds in the structural models are highlighted with red color. STM images of (a−f) are acquired with I_t = 20 pA, V_b = 1.0 V. STM image of (g) is acquired with I_t = 40 pA, V_b = 0.5 V.

networks, exhibiting distinct pore involving features (Figure 1b). Finally, the porous networks dominate the whole surface, as shown in Figure 1c (preparation temperature: 340 °C).

The temperature-induced successive phase evolution from long-range ordered self-assembly islands to the porous networks points to a thermally triggered surface chemical reaction (Figure 1a−c). Figure 1d gives a fraction of STM image zoomed from Figure 1a. The smooth density of state (DOS) and the seamless STM morphology of the product indicate selective *ortho-ortho* coupling of THPBs (the structural model is given in the lower panel). Figure 1e (zoomed from Figure 1b) discloses a ribbon-like island constructed with parallel aligned pores prepared at relatively higher temperature (320 °C). One can recognize that the pores are built up by the homocoupling of pairs of reactants. Such a conclusion is further supported by the presence of dimer products (Figure 1f). Upon further increasing the preparation temperature (340 °C), almost all *ortho* C−H bonds are activated, leading to the formation of two-dimensional polyphenylene frameworks (Figure 1g). The *ortho-ortho* coupling of phenols after annealing is in excellent agreement with the knowledge that the hydroxyl group is *ortho,para*-directing.[25] Most importantly, it is found that the irregular phase arises from the monoselective *ortho* C−H activation at lower preparation temperature, whereas the porous networks are a result of the diselective *ortho* C−H activation through the second dehydrogenation at a higher preparation temperature. The structural evolutions can therefore be attributed to the successive breaking of the *ortho* C−H bonds.

Similar porous networks on surfaces have been obtained in previous work by a Ullmann reaction or a cyclotrimerization of functional terminals.[26−28] The pore-to-pore distance of our measurements (7.4 Å) is in excellent agreement with those reported in the previous studies (7.4 Å), thus confirming our structural model (lower panel of Figure 1g). Note that no oxygen atoms are considered in this model since the limited space encompassed by the pores cannot accommodate these atoms. Actually, the O atoms are expected to dissociate upon annealing[29,30] and the deoxygenation of our samples is indeed evidenced by XPS measurements at elevated temperatures (*vide infra*).

The reaction scenario of phenols on Ag(111) is distinctively different from that on the Au(111) surface. The initial state, however, is rather similar: Deposition of THPB on Ag(111) kept at RT (Figure 2a) forms a self-assembly structure, which differs slightly from its counterpart on Au(111) (Figure S1). For samples prepared at 300 °C, the self-assembly structure decomposes into an irregular network as shown in Figure 2b, which is similar to that for THPB on Au(111) prepared at 260 °C (Figure 1a). The polymeric structure obtained from the corresponding highly resolved STM image (Figure 2c) illustrates a shoulder-shoulder jointing of the phenyls, as shown by the structural model in the inset of Figure 2c and d. Surprisingly, the surface does not favor any further structural transformation upon annealing the substrate at temperatures up to 400 °C, indicating that the second *ortho* dehydrogenation of phenols is inhibited on the Ag(111) surface. The dramatic different reaction performance of THPB indicates a surface-controlled di- and monoselective *ortho* C−H activation on Au(111) and Ag(111), respectively.

In order to unravel the mechanism of the surface-controlled reactions, extensive DFT calculations were carried out. As the phenolic proton is acidic, the phenol molecules exist on the
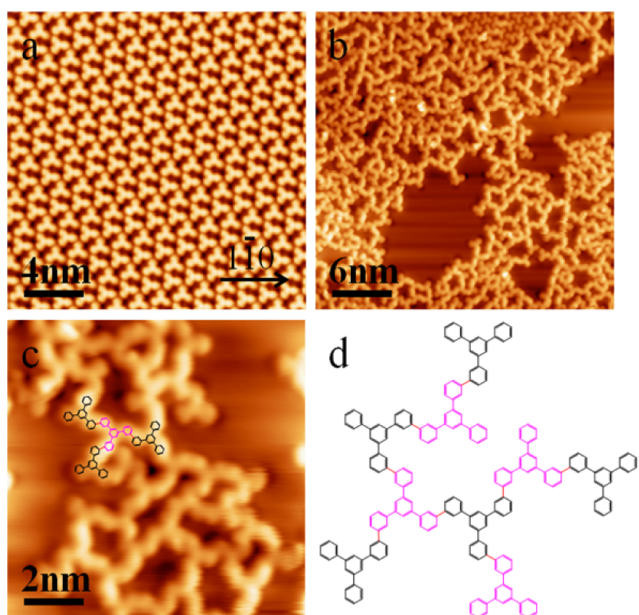
Figure 2. Reaction behaviors of THPB on Ag(111) surfaces. (a) STM image after RT deposition of THPB onto a Ag(111) surface. (b,c) Representative STM images for a sample preparation temperature of 300 °C on Ag(111). (d) Structural model of (c). STM images are acquired with I_t = 100 pA, V_b = 0.6 V.

Figure 3. (a) Phenol molecule exists on the metal surfaces in the form of phenoxyl radicals after gentle annealing. The phenoxyl radical undergoes *enol-keto* tautomerism, in which the unpaired electron may locate at the oxygen atom or an *ortho*-carbon atom. (b,c) Reaction pathways of *ortho*-dehydrogenation via the *keto* form intermediate state on Au(111) surface and Ag(111) surface, respectively. Corresponding energy profile is shown in the lower panel of respective figures.

metal surfaces in the form of phenoxyl radical after gentle annealing. This has been demonstrated by different research groups, both in solution[25] and under UHV.[31−33] Therefore, as a starting point for the DFT calculations, those phenoxyl radicals are used to represent the initial state (IS). As shown in Figure 3a, the phenoxyl radical exists in the *keto* resonance structure for which the unpaired electron is located on an *ortho*-carbon. On both gold and silver surfaces, this *ortho*-carbon can be attacked by a metal adatom with the energy barrier of about 0.30 eV, and results in a *keto*-form intermediate structure (Figure 3b). Subsequently, the first *ortho* dehydrogenation occurs with a fairly low activation barrier of 1.67 and 1.39 eV on the Au(111) surface and Ag(111) surface, respectively (Figure 3). Note that Xu et al.[24] reported an activation barrier of 1.70 eV for the C−H bond of pristine quaterphenyl on the active Cu(110) surface, and a reaction like this can hardly be accomplished on gold and silver surfaces. The *ortho-ortho* coupling then takes place to produce a dimer (IS in Figure 4).

DFT calculations reveal that the dimer molecule adopts a flat conformation on both surfaces. As a consequence, the second *ortho* dehydrogenation through the *keto*-form intermediate becomes sterically hindered. Consequently, a metal adatom approaching the dimer will first bond to the oxygen atom of the molecule as shown in Figure 4. In the initial state, the adatom attacks either the second *ortho*-carbon atom, leading to a dehydrogenation reaction, or the α-carbon atom, resulting in the reductive deoxygenation reaction. On Au(111) surfaces (Figure 4a), the activation barrier for the second *ortho* dehydrogenation is 1.80 eV, which is 0.56 eV lower than that for the C−O cleavage (2.36 eV), indicating a preference of the second *ortho* dehydrogenation reaction. The subsequent *ortho-ortho* coupling reactions, therefore, result in the formation of porous networks (Figure 1c). It is noteworthy that the increase of activation barrier from 1.67 eV for the first *ortho* dehydrogenation to 1.80 eV for the second one is in nice agreement with the temperature induced structural evolution
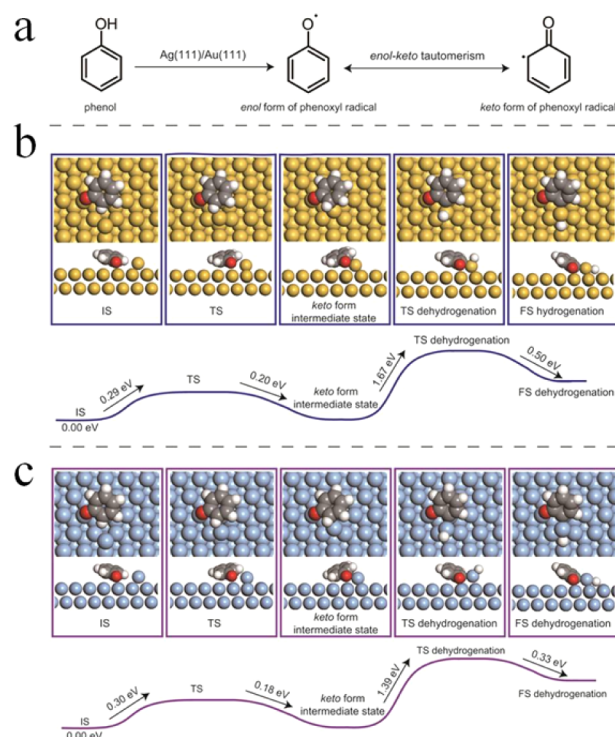
on Au(111) (Figure 1a−c). In contrast, on Ag(111), the deoxygenation reaction (activation barrier is 1.87 eV) is preferred to the second *ortho* dehydrogenation reaction (activation barrier is 2.26 eV) (Figure 4b). The lower activation energy of deoxygenation on Ag(111) can be ascribed to (i) in the IS of Figure 4b, the C−O bond is weakened by the relatively strong Ag_{surf}−O interaction; (ii) the transition state is stabilized by the Ag_{adatom}−O attractive interaction. The detailed structural evolution from IS to FS along the reaction coordinates can be seen in Figure S2 (the second dehydrogenation reaction) and Figure S3 (the deoxygenation reaction). After the deoxygenation reactions on Ag(111), further *ortho* C−H bond activation and aryl−aryl coupling are suppressed. Note that the Boltzmann factor between the dehydrogenation and deoxygenation at 250 °C is 2.6×10^5 and 1.7×10^{-4} for Au(111) and Ag(111), respectively, leading to that stunning reaction selectivity regarding mono- and di-*ortho* C−H activation. Indeed, the second *ortho* dehydrogenation was not observed on Ag(111) surfaces experimentally (Figure 2).

The respective reaction pathways are further clarified by XPS measurements. After deposition of THPB on Au(111) at RT, the C 1s region exhibits two prominent peaks as displayed in Figure 5a. The main peak centered at a binding energy (BE) of 284.3 eV is ascribed to the C−C bonds, whereas the second one centered at 285.9 eV is attributed to the C−O bonds.[32,33] Regarding the O 1s region, there is a sole peak centered at 533.2 eV observable, which is ascribed to the hydroxyl groups of pristine THPB[31−33] (Figure 5a). Upon annealing the sample at 150 °C, the intensity of this peak decreases and a new feature centered at 531.0 eV emerges, which is associated with the
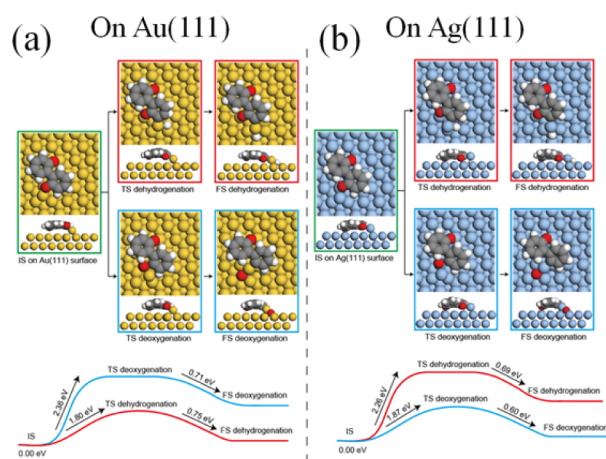
Figure 4. DFT calculations of the reaction pathways for the second *ortho*-dehydrogenation and reductive oxygenation reactions on the (a) Au(111) surface and (b) Ag(111) surfaces. Corresponding energy profile is shown in the lower panels of the respective figures. In the initial states of dehydrogenation and deoxygenation reactions, a metal adatom is sitting above a hollow site near one of the oxygen atoms. In the transition states, the metal adatom tends to squeeze itself into the nearest CH single bond (dehydrogenation) or the CO double bond (deoxygenation), and thus elongates the bond-length of the CH and the carbonyl group, respectively. In the final states, the metal adatoms are inserted into the CH bonds (dehydrogenation) and the CO bonds (deoxygenation). Over the Au(111) surface, the energy barrier of dehydrogenation is 0.56 eV lower than that of the deoxygenation reaction. Over the Ag(111) surface, by contrast, the activation energy of dehydrogenation reaction is 0.39 eV higher than that of the deoxygenation reaction.
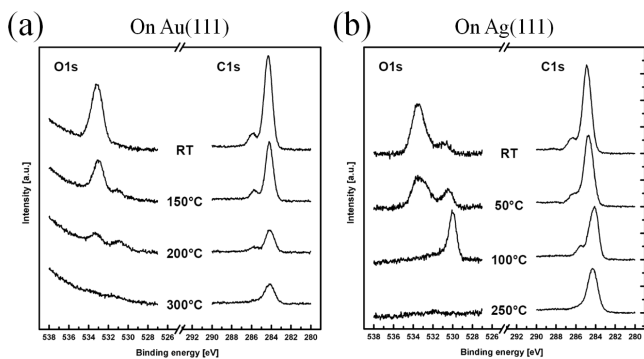

Figure 5. O 1s and C 1s line scan of the X-ray photoelectron spectra on (a) Au(111) and (b) Ag(111) surfaces. The sample preparation temperature is indicated between the spectra.

formation of carbonyl groups.[31−33] A further increase of the substrate temperature to 200 °C leads to the enhancement of the relative intensity of the carbonyl-derived peak (531.0 eV), suggesting that the hydroxyls are gradually converted to carbonyls at elevated temperatures. Moreover, at an even higher annealing temperature of 300 °C, the O 1s signal virtually vanishes, providing evidence of a deoxygenation process as proposed above. The XPS results for Ag(111) are rather similar to those obtained for Au(111) (Figure 5b). Again, the corresponding C 1s region exhibits two peaks at 284.9 and 286.4 eV which are ascribed to the C−C and C−O bonds, respectively. Concerning the O 1s region, a comparable hydroxyl-related component centered at 533.5 eV O 1s can be observed. However, in contrast to the data obtained for Au(111), two major differences are apparent. First, a carbonyl

signal at 531.1 eV is already visible at RT and it increases successively with increasing temperature, becoming the dominant component at 100 °C. The partial conversion of hydroxyls to carbonyls at RT may be the origin of the slight difference between the respective self-assembly structures on both substrates at RT (Figure S1a and 2a). Second, the oxygen signal vanishes already at a temperature of 250 °C, i.e., at a lower annealing temperature than in the case of Au(111) (300 °C), thus confirming the favorable deoxygenation reaction on Ag(111) surfaces as anticipated by the DFT calculations. It is worth noting that an obvious shift was observed on the low energy peak of O 1s spectra. The bonding energy shifts from 531.1 eV at RT to 530.4 eV at 50 °C and to 530.1 eV at 100 °C. This can be explained by the phase evolution of the self-assembly structure at different preparation temperature (see Figure S4 for details), which leads to the different local environment of the chemical species. Actually such a phenomenon is quite common and similar peak shifting has been reported by several groups.[26,30,31]

In order to demonstrate the generality of the surface-controlled mono/diselective *ortho* C−H activation, complementary to our studies on THPB, the reaction behavior of DHQP on both Au(111) and Ag(111) was investigated. The deposition of DHQP on Au(111) kept at a relatively low temperature (270 °C) leads predominantly to the formation of stripes (Figure S5a). High resolution STM images reveal that the phenyl rings are joined together via an *ortho-ortho* coupling (Figure S5b). Similar to the reactivity of THPB on Au(111), DHQPs form two-dimensional networks at a higher preparation temperature (320 °C), as shown in Figure 6a (further
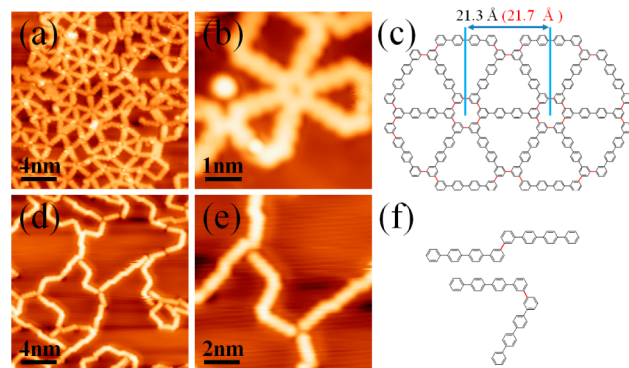

Figure 6. Reaction behaviors of DHQP on gold and silver surfaces. (a,b) STM image for the sample preparation temperature of 320 °C on Au(111). (c) Structural model of (a). Black and red numbers show the experimental and calculated pore-to-pore distances, respectively. (d,e) STM image for a sample preparation temperature of 300 °C on Ag(111). (f) Structural model of (d). Newly formed bonds are highlighted by red color in (c) and (f). (a) is acquired with I_t = 20 pA, V_b = 1.0 V. (b) is acquired with I_t = 20 pA, V_b = 0.5 V. (c) and (d) are acquired with I_t = 100 pA, V_b = 0.1 V.

evidence can be found in Figure 6b and Figure S5d). The pore-to-pore distance measured experimentally is 21.3 Å, which is consistent with the calculated result (21.7 Å), thus supporting the validity of the proposed structural model (Figure 6c). Analogously to THPB (Figure 1c), the formation of porous networks provides unassailable evidence of the diselective *ortho* C−H activation on Au(111) surface.

Again, the reaction behavior of DHQP is rather different on Ag(111). After deposition of DHQP at 300 °C, chain-like

structures are observed (Figure 6d). The reaction performance nicely resembles that of THPB (Figure 2) with regard to the following aspects: (i) High resolution images (Figure 6d and e) reveal *ortho-ortho* coupling of DHQP monomers. The corresponding structural model is displayed in Figure 6f. (ii) The 1D structure remains unaltered at temperatures up to 400 °C. The STM studies strongly suggest that the second *ortho*-dehydrogenation of DHQP is withheld on Ag(111).

Moreover, those novel reaction pathways work not only for homocoupling, but also for cross-coupling of two different monomers. Indeed, the surface-assisted cross-coupling of THPB and DHQP via selective *ortho* C−H activation are successfully achieved on both gold and silver surfaces (Figure S6).

CONCLUSIONS

In summary, we have successfully achieved selective *ortho*−*ortho* coupling on metal surfaces and the C−H bond activation barrier is reduced dramatically through the introduction of hydroxyl directing groups to the precursors. More importantly, the unprecedented surface-controlled mono- and diselective *ortho* C−H activations are discovered. By thorough STM studies, combining with XPS measurements and DFT calculations, we have elucidated the respective reaction pathways. The activation barriers for the first *ortho* dehydrogenation reaction on Au(111) and Ag(111) are both lowered by the formation of stable *keto*-form intermediate structures. In the next step a subsequent catalytic reductive deoxygenation reaction is preferred over the second *ortho* dehydrogenation on Ag(111). On Au(111), however, the opposite is the case, which results in the surface-controlled reaction selectivity. Thus, our findings provide an excellent generic route for surface-assisted aryl−aryl coupling through mono/diselective *ortho* C−H bond activation.

METHODS

STM Measurements. All STM measurements were performed in an ultrahigh vacuum (UHV) system (base pressure better than 1×10^{-10} Torr). Experiments were conducted with commercial Unisoku low temperature scanning tunneling microscopy (LT-STM 1500s). All the STM measurements are performed at a temperature of 77 K. The Au(111) and Ag(111) substrates were cleaned by repeated cycles of argon ion sputtering and annealing before the deposition of organic molecules. A commercial Pt−Ir tip was carefully prepared by e-beam heating. The STM images were analyzed using WsXM.

XPS Measurements. All X-ray photoemission spectroscopy (XPS) measurements were carried out in a different UHV chamber (base pressure 1×10^{-10} mbar). The respective XPS setup consists of a monochromatic X-ray source providing Al Kα radiation ($\hbar\omega$ = 1486.6 eV) and a high-resolution hemispherical electron analyzer (Specs GmbH, Phoibos 150) for photoelectron detection. The Au(111) and Ag(111) substrates were cleaned by repeated cycles of argon ion sputtering and annealing before THPB deposition. The latter was carried out on the substrates kept at room temperature. Subsequently, the samples were annealed for 20 mins at each desired temperature by electron bombardment. The particular sample temperature was measured by means of a thermocouple temperature sensor attached to the sample holder of the manipulator.

DFT Calculations. Density functional theory (DFT) calculations were performed using the VASP code[34,35] and the projector augmented wave (PAW) method[36] and GGA-PBE functional.[37] The effect of van der Waals (vdW) interactions was included with the vdw-DF method. Au(111) and Ag(111) surfaces were modeled using periodic slabs, consisting of four atomic layers and a vacuum thickness of 20 Å. The topmost two atomic layers of metal atoms and the molecules were allowed to relax in three dimensions. All structures are fully relaxed until the force on each atom is smaller than 0.01 eV per Angstrom. The transition states were determined by the climbing image nudged-elastic band (CI-NEB) method. Three structural images were inserted between the initial states and the final states in all CI-NEB calculations. The Brillouin zone (BZ) sampling was done using a $2 \times 2 \times 1$ Monkhorst−Pack grid for all calculations.

Molecular Synthesis. 1,3,5-Tris(4-hydroxyphenyl)benzene (THPB) and [1,1′:4′,1″:4″,1‴-quaterphenyl]-4,4‴-diol (DHQP) were synthesized by applying methods reported previously.[38,39]

ASSOCIATED CONTENT

Ⓢ Supporting Information

The Supporting Information is available free of charge on the ACS Publications website at DOI: 10.1021/jacs.5b13286.

Self-assembly of THPB on Au(111) surface; DFT calculations of the deoxygenation reaction and the second *ortho* dehydrogenation; Structural evolution of DHQP on Au(111) surface; Cross-coupling of phenol derivatives on Au(111) and Ag(111) surfaces (PDF)

AUTHOR INFORMATION

Corresponding Authors
*jianfan@suda.edu.cn.
*chilf@suda.edu.cn.
Author Contributions
‡Qing Li, Biao Yang, and Haiping Lin contributed equally.
Notes
The authors declare no competing financial interest.

ACKNOWLEDGMENTS

REFERENCES

(1) Arndtsen, B. A.; Bergman, R. G.; Mobley, T. A.; Peterson, T. H. *Acc. Chem. Res.* **1995**, *28*, 154−162.
(2) Bringmann, G.; Gulder, T.; Gulder, T. M.; Breuning, M. *Chem. Rev.* **2011**, *111*, 563−639.
(3) Zwaneveld, N. A. A.; Pawlak, R.; Abel, M.; Catalin, D.; Gigmes, D.; Bertin, D.; Porte, L. *J. Am. Chem. Soc.* **2008**, *130*, 6678−6679.
(4) Lin, T.; Shang, X. S.; Adisoejoso, J.; Liu, P. N.; Lin, N. *J. Am. Chem. Soc.* **2013**, *135*, 3576−3582.
(5) Gourdon, A. *Angew. Chem., Int. Ed.* **2008**, *47*, 6950−6953.
(6) Matena, M.; Riehm, T.; Stöhr, M.; Jung, T. A.; Gade, L. H. *Angew. Chem., Int. Ed.* **2008**, *47*, 2414−2417.
(7) Perepichka, D. F.; Rosei, F. *Science* **2009**, *323*, 216−217.

(8) Fan, Q. T.; Wang, C. C.; Han, Y.; Zhu, J. F.; Hieringer, W.; Kuttner, J.; Hilt, G.; Gottfried, J. M. *Angew. Chem., Int. Ed.* **2013**, *52*, 4668−4672.

(9) Liu, X. H.; Guan, C. Z.; Ding, S. Y.; Wang, W.; Yan, H. J.; Wang, D.; Wan, L. J. *J. Am. Chem. Soc.* **2013**, *135*, 10470−10474.

(10) Li, Q.; Han, C. B.; Fuentes-Cabrera, M.; Terrones, H.; Sumpter, B. G.; Lu, W. C.; Bernholc, J.; Yi, J. Y.; Gai, Z.; Baddorf, A. P.; Maksymovych, P.; Pan, M. H. *ACS Nano* **2012**, *6*, 9267−9275.

(11) Li, Q.; Owens, J. R.; Han, C. B.; Sumpter, B. G.; Lu, W. C.; Bernholc, J.; Meunier, V.; Maksymovych, P.; Fuentes-Cabrera, M.; Pan, M. H. *Sci. Rep.* **2013**, *3*, 2102.

(12) Grill, L.; Dyer, M.; Lafferentz, L.; Persson, M.; Peters, M. V.; Hecht, S. *Nat. Nanotechnol.* **2007**, *2*, 687−691.

(13) Zhang, Y. Q.; Kepčija, N.; Kleinschrodt, M.; Diller, K.; Fischer, S.; Papageorgiou, A. C.; Allegretti, F.; Björk, J.; Klyatskaya, S.; Klappenberger, F.; Ruben, M.; Barth, J. V. *Nat. Commun.* **2012**, *3*, 1286.

(14) Zhang, H. M.; Lin, H. P.; Sun, K. W.; Chen, L.; Zagranyarski, Y.; Aghdassi, N.; Duhm, S.; Li, Q.; Zhong, D. Y.; Li, Y. Y.; Mullen, K.; Fuchs, H.; Chi, L. F. *J. Am. Chem. Soc.* **2015**, *137*, 4022−4025.

(15) Zhong, D. Y.; Franke, J. H.; Podiyanachari, S. K.; Blömker, T.; Zhang, H. M.; Kehr, G.; Erker, G.; Fuchs, H.; Chi, L. F. *Science* **2011**, *334*, 213−216.

(16) Chen, Y. C.; de Oteyza, D. G.; Pedramrazi, Z.; Chen, C.; Fischer, F. R.; Crommie, M. F. *ACS Nano* **2013**, *7*, 6123−6128.

(17) Cai, J. M.; Ruffieux, P.; Jaafar, R.; Bieri, M.; Braun, T.; Blankenburg, S.; Muoth, M.; Seitsonen, A. P.; Saleh, M.; Feng, X. L.; Müllen, K.; Fasel, R. *Nature* **2010**, *466*, 470−473.

(18) Narita, A.; Feng, X. L.; Hernandez, Y.; Jensen, S. A.; Bonn, M.; Yang, H. F.; Verzhbitskiy, I. A.; Casiraghi, C.; Hansen, M. R.; Koch, A. H. R.; Fytas, G.; Ivasenko, O.; Li, B.; Mali, K. S.; Balandina, T.; Mahesh, S.; De Feyter, S.; Mullen, K. *Nat. Chem.* **2013**, *6*, 126−132.

(19) Treier, M.; Pignedoli, C. A.; Laino, T.; Rieger, R.; Müllen, K.; Passerone, D.; Fasel, R. *Nat. Chem.* **2011**, *3*, 61−67.

(20) Haq, S.; Hanke, F.; Sharp, J.; Persson, M.; Amabilino, D. B.; Raval, R. *ACS Nano* **2014**, *8*, 8856−8870.

(21) Wiengarten, A.; Seufert, K.; Auwarter, W.; Ecija, D.; Diller, K.; Allegretti, F.; Bischoff, F.; Fischer, S.; Duncan, D. A.; Papageorgiou, A. C.; Klappenberger, F.; Acres, R. G.; Ngo, T. H.; Barth, J. V. *J. Am. Chem. Soc.* **2014**, *136*, 9346−9354.

(22) Eichhorn, J.; Heckl, W. M.; Lackinger, M. *Chem. Commun.* **2013**, *49*, 2900−2902.

(23) In't Veld, M.; Iavicoli, P.; Haq, S.; Amabilino, D. B.; Raval, R. *Chem. Commun.* **2008**, 1536−1538.

(24) Sun, Q.; Zhang, C.; Kong, H. H.; Tan, Q. G.; Xu, W. *Chem. Commun.* **2014**, *50*, 11825−11828.

(25) Lee, Y. E.; Cao, T.; Torruellas, C.; Kozlowski, M. C. *J. Am. Chem. Soc.* **2014**, *136*, 6782−6785.

(26) Yang, B.; Bjork, J.; Lin, H. P.; Zhang, X. Q.; Zhang, H. M.; Li, Y. Y.; Fan, J.; Li, Q.; Chi, L. F. *J. Am. Chem. Soc.* **2015**, *137*, 4904−4907.

(27) Bieri, M.; Nguyen, M. T.; Gröning, O.; Cai, J. M.; Treier, M.; Aït-Mansour, K.; Ruffieux, P.; Pignedoli, C. A.; Passerone, D.; Kastler, M.; Müllen, K.; Fasel, R. *J. Am. Chem. Soc.* **2010**, *132*, 16669−16676.

(28) Zhou, H. T.; Liu, J. Z.; Du, S. X.; Zhang, L. Z.; Li, G.; Zhang, Y.; Tang, B. Z.; Gao, H. J. *J. Am. Chem. Soc.* **2014**, *136*, 5567−5570.

(29) Kawai, S.; Eren, B.; Marot, L.; Meyer, E. *ACS Nano* **2014**, *8*, 5932−5938.

(30) Fischer, S.; Papageorgiou, A. C.; Lloyd, J. A.; Oh, S. C.; Diller, K.; Allegretti, F.; Klappenberger, F.; Seitsonen, A. P.; Reichert, J.; Barth, J. V. *ACS Nano* **2014**, *8*, 207−215.

(31) Giovanelli, L.; Ourdjini, O.; Abel, M.; Pawlak, R.; Fujii, J.; Porte, L.; Themlin, J.; Clair, S. *J. Phys. Chem. C* **2014**, *118*, 14899−14904.

(32) Bebensee, F.; Svane, K.; Bombis, C.; Masini, F.; Klyatskaya, S.; Besenbacher, F.; Ruben, M.; Hammer, B.; Linderoth, T. R. *Chem. Commun.* **2013**, *49*, 9308−9310.

(33) Bebensee, F.; Svane, K.; Bombis, C.; Masini, F.; Klyatskaya, S.; Besenbacher, F.; Ruben, M.; Hammer, B.; Linderoth, T. R. *Angew. Chem., Int. Ed.* **2014**, *53*, 12955−12959.

(34) Kresse, G.; Furthmuller, J. *Comput. Mater. Sci.* **1996**, *6*, 15−50.

(35) Kresse, G.; Furthmuller, J. *Phys. Rev. B: Condens. Matter Mater. Phys.* **1996**, *54*, 11169−11186.

(36) Kresse, G.; Joubert, D. *Phys. Rev. B: Condens. Matter Mater. Phys.* **1999**, *59*, 1758−1775.

(37) Perdew, J. P.; Burke, K.; Ernzerhof, M. *Phys. Rev. Lett.* **1996**, *77*, 3865−3868.

(38) Yamaguchi, I.; Sato, K.; Okuno, M. J. *J. Phys. Org. Chem.* **2014**, *27*, 622−627.

(39) Ung, V. A.; Bardwell, D. A.; Jeffery, J. C.; Maher, J. P.; McCleverty, J. A.; Ward, M. D.; Williamson, A. *Inorg. Chem.* **1996**, *35*, 5290−5299.